# Role of β-Hairpin Formation in Aggregation: The Self-Assembly of the Amyloid-β(25–35) Peptide

Luca Larini and Joan-Emma Shea*

Department of Chemistry and Biochemistry, and Department of Physics, University of California, Santa Barbara, California

ABSTRACT   The amyloid-β(25–35) peptide plays a key role in the etiology of Alzheimer's disease due to its extreme toxicity even in the absence of aging. Because of its high tendency to aggregate and its low solubility in water, the structure of this peptide is still unknown. In this work, we sought to understand the early stages of aggregation of the amyloid-β(25–35) peptide by conducting simulations of oligomers ranging from monomers to tetramers. Our simulations show that although the monomer preferentially adopts a β-hairpin conformation, larger aggregates have extended structures, and a clear transition from compact β-hairpin conformations to extended β-strand structures occurs between dimers and trimers. Even though β-hairpins are not present in the final architecture of the fibril, our simulations indicate that they play a critical role in fibril growth. Our simulations also show that β-sheet structures are stabilized when a β-hairpin is present at the edge of the sheet. The binding of the hairpin to the sheet leads to a subsequent destabilization of the hairpin, with part of the hairpin backbone dangling in solution. This free section of the peptide can then recruit an extra monomer from solution, leading to further sheet extension. Our simulations indicate that the peptide must possess sufficient conformational flexibility to switch between a hairpin and an extended conformation in order for β-sheet extension to occur, and offer a rationalization for the experimental observation that overstabilizing a hairpin conformation in the monomeric state (for example, through chemical cross-linking) significantly hampers the fibrillization process.

## INTRODUCTION

Amyloidosis refers to a family of diseases characterized by the presence of extracellular proteinaceous aggregate deposits known as amyloids. These diseases can target different organs, and even though the deposits originate from different proteins, they share a number of common structural features (1–4), including the ability to bind to amyloid dyes and a characteristic x-ray diffraction pattern corresponding to the presence of a cross-β-sheet structure (4–9).

Alzheimer's disease (10) (AD) is perhaps the best-known amyloid disorder and is characterized by the aggregation of amyloid-β proteins (Aβ) in the brain (11). Aβ proteins are proteolytic byproducts of the amyloid precursor protein (APP) (12). Cleavage of this transmembrane protein gives rise to protein fragments of varying length (13), the most common of which are the 40- or 42-residues-long Aβ(1–40) and Aβ(1–42) peptides (14). The aggregation of these peptides is associated with neuronal death and resulting dementia (6,7,15,16). The mechanism by which aggregation leads to cell death remains a matter of debate, and toxicity has been associated with both small oligomers and full-fledged fibrils (17–19). Of interest, some aggregates show greater toxicity after aging (15). This may be due to either a change in structural arrangement (5,9,20) or to the fact that the original aggregate undergoes major chemical modifications (20,21) that produce several, smaller (possibly more toxic) species (14).

Although the Aβ(1–40) and Aβ(1–42) peptides are the most abundant forms of Aβ produced in the body, aggregates of shorter fragments are also observed in brain tissue. In this study we focused on the aggregation process of one such fragment, the 11-amino-acid GSNKGAIIGLM peptide corresponding to the 25–35 segment of the longer Aβ peptides (15,19,21–24). This amphiphilic fragment corresponds to the transmembrane segment of APP (25), with the C-terminus inserted into the membrane in the context of APP.

Among the many fragments of Aβ that have been studied experimentally, Aβ(25–35) represents the smallest naturally occurring fragment that retains both the toxicity and the aggregation properties of the full-length molecule (15,19,26). These properties make it a useful proxy for studying the aggregation of the full-length Aβ peptides, and more generally for elucidating the formation of other amyloid fibers and their toxicity (14,19,27–31).

As is the case with the full-length Aβ peptide, Aβ(25–35) is an intrinsically disordered peptide (IDP). In other words, it does not possess a well-defined structure, and instead tends to populate multiple conformations. These peptides are extremely difficult to characterize in water, and their disordered nature, low solubility, and high tendency to aggregate make it very challenging to achieve a structural characterization through standard ensemble averaging techniques such as NMR. For this reason, no definitive, experimentally obtained three-dimensional structure of the Aβ(25–35) monomer in water has been obtained. Experiments have been conducted in water mixtures or in micellar solution (32,33), and it has been shown that this peptide

adopts different conformations and fibril morphologies under different experimental conditions (27,28,31–36).

The most detailed atomistic pictures of the very early stages of aggregation have been obtained by means of simulations. The latter enable a single-molecule characterization of the conformations adopted by the peptide and hence are well suited to characterize the conformations of IDPs. An early study by Wei and Shea (37) showed that the monomeric state of Aβ(25–35) adopts a β-hairpin conformation in water, and a helical conformation in lipid mimicking solvents (the latter in agreement with experimental data). In a subsequent study of dimers of Aβ(25–35) in water, Wei et al. (38) showed that the dimers could adopt a number of conformations in which the Aβ(25–35) peptide could adopt a hairpin (in similarity to the monomeric case) or undergo a structural rearrangement so as to adopt an extended strand conformation. This rearrangement was later confirmed in simulations by Kittner and Knecht (39).

It is intriguing that although β-hairpins are observed in simulations of monomers of a number of aggregating peptides (including various fragments of the Aβ peptides, as well as other peptides, such as the IAPP peptide implicated in Type II diabetes), hairpins are not seen in the fibril structures of these peptides (37,38,40–63). Rather, the peptides appear to prefer either extended conformations or strand-loop-strand conformations in the context of fibrils. In this work, we extend our earlier simulations on monomers and dimers of Aβ(25–35) to larger aggregates, with the goal of understanding the role of β-hairpin formation in early aggregation. We consider both trimer and tetramer formation, and analyze the structural modifications that occur during the aggregation process. Emphasis is placed on noteworthy structural features that are critical for triggering and sustaining the aggregation process. The replica-exchange protocol we used does not directly provide information about the pathways or kinetics of aggregation, but does enable a thorough characterization of the thermodynamics of aggregation. We will discuss our results in terms of the structures obtained, starting from monomer to tetramer. Presenting the results in this order allows an appreciation of how the same interactions that at the very beginning favor a β-hairpin structure for the monomer lead to β-sheet structures in larger aggregates composed of fully extended chains, with only a minor population of β-hairpins. For this particular peptide, the trimer emerges as the critical oligomeric size in the transition from β-hairpin dominant to β-sheet dominant conformations. The common physical interactions that are responsible for stabilizing both a β-hairpin conformation and β-sheet structures under different conditions explain the essential role that monomers play in stabilizing and propagating the growth front of the fibril. We show that a β-hairpin (the most common monomeric conformation) residing at the edge of a growing β-sheet can prevent the sheet from collapsing into more compact conformations (with the latter being less likely to grow

into full-fledged fibrils). This hairpin can then subsequently extend into a β-strand conformation, allowing the β-sheet to grow through the inclusion of other monomers from solution.

## METHODS

The simulation approach is summarized below. A detailed description of the simulation protocol, convergence, and equilibration can be found in the Supporting Material. We collected all of the data in the canonical NVT ensemble using the package GROMACS (64–67) and the OPLS-AA force field (68–70) in association with the TIP3P water model (71). For the simulations in solution, we computed the electrostatic interactions using the particle mesh Ewald method (72,73) with a real-space cutoff of 1.2 nm. The same cutoff was used to compute the van der Waals interactions as well as long-range dispersion corrections for both energy and pressure. The temperature was kept constant by a Nosé-Hoover thermostat (74–76) and the equations of motion were integrated by means of the leap-frog algorithm (77) with a time step of 2 fs. Constraints were used for the heavy atoms connected to hydrogens atoms, with the LINCS (78) algorithm for the protein and the SETTLE (79) algorithm for water. The edge of the box of water was ~5.4 nm long (see Supporting Material) and periodic boundary conditions were employed.

As discussed in the Introduction, small peptides do not have a preferential, native conformation, and instead populate multiple states. Therefore, we employed replica-exchange molecular dynamics (REMD) to improve the sampling efficiency (80–82). This method consists of running multiple simulations of the same system in parallel but at different temperatures. At regular intervals of 3 ps, conformations at different temperatures are compared and eventually swapped according to their difference in energy. The temperature ranges were as follows: 290–497.4 K (monomer), 290–356 K (dimer), and 290–411 K (trimer and tetramer). To achieve proper sampling and statistic, simulations were run for 206 ns (monomer), 330 ns (dimer), 502 ns (trimer), and 517 ns (tetramer). The initial 107 ns (monomer), 123 ns (dimer), 207 ns (trimer), and 208 ns (tetramer) were discarded as equilibration data.

We analyzed the data using the tools provided with the GROMACS package. In particular, cluster analysis was performed with the use of the Daura algorithm (83), which constructs clusters based on the root mean-square deviation (RMSD) of the peptide. The RMSD was computed only for the backbones (excluding the terminal groups), and structures with RMSD within a specified cutoff were collected inside the same cluster. The cutoff employed was different for each case and is reported when applicable. The relative abundance of each cluster is reported in Fig. S5, Fig. S6, Fig. S7, and Fig. S8. In the text, we limit ourselves to discussing clusters that either have a relative abundance of >5% or present notable features.

## RESULTS

### Monomer: collapsed coils coexist with hairpin-like β-turn structures

As in our earlier work, we find that the monomeric state of the Aβ(25–35) fragment populates mainly conformations that can be classified as collapsed coil and hairpin-like β-turn (37). The radius of gyration and the end-to-end distance are highly correlated (see Fig. S9), and the ratio of these quantities ranges between 2.5 and 3.3 (Fig. S9) (and thus is much smaller than the Gaussian chain value of 6 (84)). These features highlight the fact that the chain strongly prefers to adopt compact conformations, and that extended conformations (as would be seen in a fibril) are not favored.

The tendency to adopt compact conformations can be explained based on the distribution of the charged groups along the backbone. The most important groups in this respect are the two termini (the protein is in its zwitterionic form, with charged glycine G25 and methionine M35) and the positively charged side chain of the lysine (K28). The majority of the conformations prefer to keep the two termini close to each other, with the side chain of K28 dangling in solution. However, in an alternate arrangement, K28 is positioned close to the M35 terminus (Fig. S10).

To clearly identify the structures adopted by the monomer A$\beta$(25–35) in solution, we performed a cluster analysis of the available conformations. The cluster analysis groups structures based on the similarity (i.e., the RMSD difference) of their backbone conformations. Clusters are then ranked according to their abundance (i.e., the number of conformations belonging to each cluster), with cluster A being the most abundant.

Fig. 1 *a* shows clusters with an abundance of >5% based on their RSMD from the reference structures A1 and B. For greater clarity, we also report these structures along with their relative abundance in Fig. S5 and Fig. S12. All of these structures have a $\beta$-hairpin conformation of the backbone, with the bend occurring at the location G29-A30-I31. Inside cluster A, one can clearly identify at least three major subpopulations, classified as A1, A2, and A3. The most populated conformation, A1, differs from the other clusters because of the formation of hydrogen bonds between glycine G29 or isoleucine I31 and asparagine N27 (Fig. S11). This hydrogen bond allows the hairpin to bend the turn region internally, so that an extremely compact conformation is obtained (Fig. S12).

The absence of the hydrogen bond with N27 leads to more planar $\beta$-hairpin conformations, as is the case in clusters A2, A3, and B. Except for cluster C, the turn region is tightly packed to maximize the number of hydrogen bonds.

All of the structures described above share a common feature in that they try to preserve a $\beta$-hairpin conformation that segregates the hydrophobic moieties on one side of the hairpin (residues 31–35). The other side of the $\beta$-hairpin is positively charged, with the positive side chain of K28 close to the positive N-terminus.

## Dimer: a majority of hairpin dimers and a minority of extended $\beta$-sheet dimers

The structure of the monomer discussed above is mainly dictated by its tendency to adopt compact conformations that maximize the number of (intramolecular) hydrogen bonds. To assess how the structure of each monomer changes when included inside a dimer, we plot in Fig. 1 *b* the probability distribution for one chain inside the dimer when the reference structures are the same as in the monomer case. As can be seen from this figure, there is a rich diversity of structures, with the majority of chains inside the dimer retaining a high population of $\beta$-hairpin structures. In addition, a smaller, new population starts to appear, corresponding to chains that are in the extended state S1.

This plot should be compared with Fig. 2 *a*, which reports the probability distribution for the structures found for the dimers. In agreement with previous studies (38,39), the dimer starts to show $\beta$-sheet structures (see cluster B). However, the majority of the clusters (see also Fig. 3) show a clear predominance of $\beta$-hairpins.
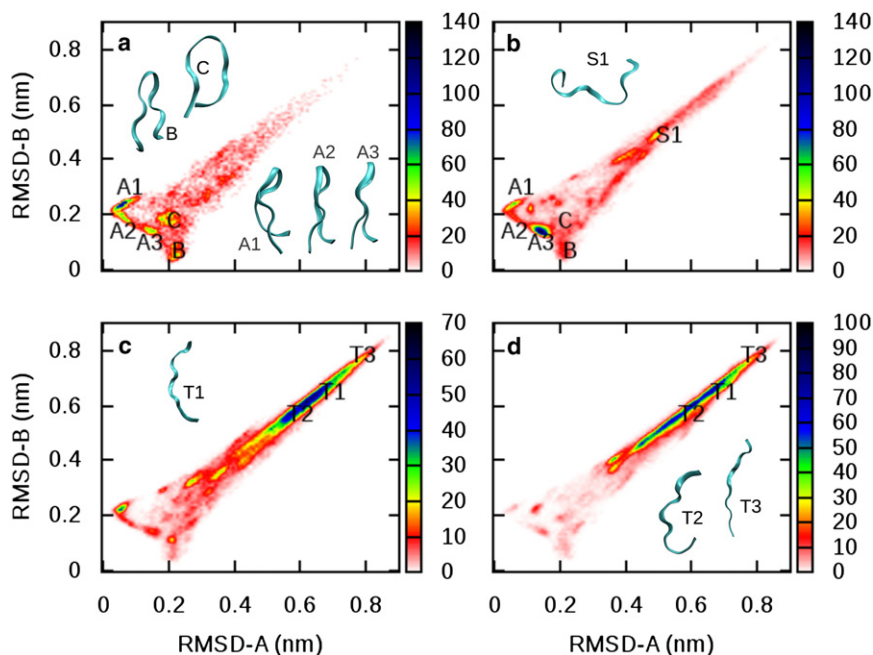


FIGURE 1 Probability of finding a particular conformation of the backbone within (*a*) monomers, (*b*) dimers, (*c*) trimers, and (*d*) tetramers. For all of the cases considered, the reference structures are taken from clusters A (*x* axis) and B (*y* axis) of the monomer. Representative conformations for the main clusters are reported as well. The cutoff used for clustering was 0.12 nm. We identified the subpopulation for cluster A by performing a second cluster analysis only on those populations with a cutoff of 0.7 nm. See also Fig. S5 and Fig. S12.
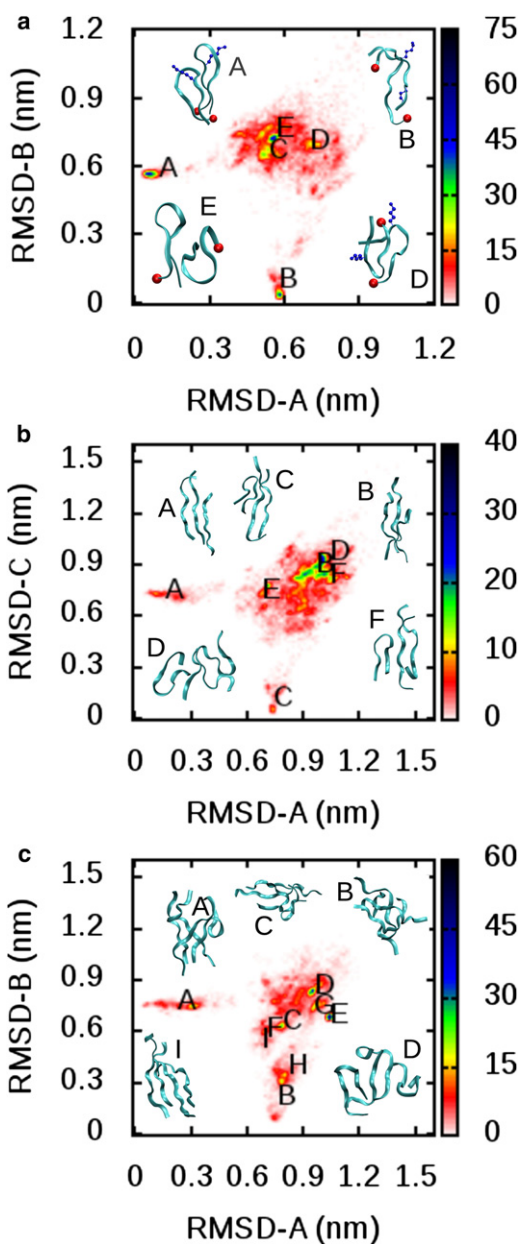
FIGURE 2 Probabilities and representative conformations for (*a*) dimers, (*b*) trimers, and (*c*) tetramers. The probability distribution was computed according to the RMSD of each conformation from the reference structures (clusters A (*x* axis) and B (*y* axis) for dimers and tetramers, and clusters A (*x* axis) and C (*y* axis) for the trimer case). The monomer case is reported in Fig. 1 *a*. The cutoffs for clustering were 0.26 nm (dimers), 0.3 nm (trimers), and 0.35 nm (tetramers). In the case of dimers, the side chain of K28 (only heavy atoms) is shown using balls and sticks and the C-terminus is located with a sphere at one end of the backbone (see text and Fig. 3 for details). Extended lists of the clusters for each case are provided in Fig. S6, Fig. S7, and Fig. S8.
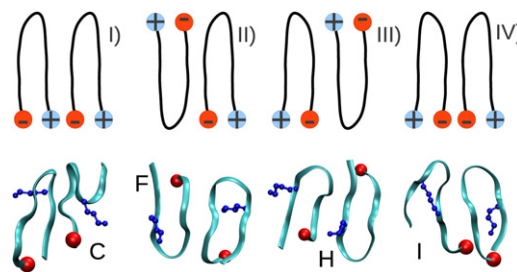


FIGURE 3 Possible arrangements of a pair of hairpins to form a planar dimer. Another set of arrangements can be constructed by switching the sign of all of the charges. For each case, a cluster from our simulations with the same arrangement is shown (see also Fig. 2 *a*).

β-hairpins (see Fig. 3) and compare them with the structures that are actually observed in our simulations. Fig. 3 shows four possible dimer constructs consisting of two β-hairpins in a planar conformation.

Case I has the terminal charges placed in an alternating conformation. This arrangement has the disadvantage of putting both the positive side chain of the lysine and the positive N-terminus in close contact with the negative terminus of the other chain. In a situation like this, the competition between the positive charges for interacting with the negative terminus destabilizes the dimer. The opposite situation can be found in case IV, where the dimer now has to contend with two charges of the same sign in close contact. This situation is unfavorable, even though the case depicted in Fig. 3 does benefit from a mild stabilization offered by the hydrophobic moieties being in proximity. The alternate case, in which two positive charges are close to each other, will be extremely unstable because now both the positive termini and K28 are in contact. Cases II and III are analogous to cases I and IV above, but with one of the peptides flipped. Case II is more favorable than case III because it benefits from the burial of the hydrophobic moieties (as in case IV).

Similar arguments explain why a perfect stacking of hairpins is not favorable and instead leads to a distorted stacking such as the one observed in our simulations in cluster D (Fig. 2 *a*). An alternate solution to the stacking problem is adopted by the conformations in clusters A and E (Fig. 2 *a*), which consists of tilting one of the two hairpins in the stacking to maximize interchain contacts and minimize electrostatic repulsions.

Because of the destabilizing effects of the charged groups, in many of the clusters found in our simulations, one of the two hairpins is usually destabilized, as in the case of clusters C and D. In this situation, one section of the chain tends to form hydrogen bonds with the other hairpin, at the same time extending the other section of the hairpin. It is not surprising to find that sometimes both hairpins are destabilized, so that they both adopt an extended conformation stabilized by interchain hydrogen bonds (38,39) as in cluster B. The two chains adopt an

antiparallel alignment that prevents charges with the same sign from being close together.

In the paragraphs above, we were able to explain the conformations found for the dimers based on electrostatic considerations. These findings lead us to conclude that at least for length scales comparable to the size of a dimer, electrostatics are the dominant driving force that dictates the prevalent structural arrangement.

We now turn to the question of whether the compact dimers are energetically or entropically stabilized. On the basis of dimer simulations, Kittner and Knecht (39) suggested that compact conformations (defined based on a radius-of-gyration cutoff) are entropically stabilized. Our simulations support this picture, and below we propose a simple argument to that effect. As shown in Fig. 1 b, dimers are mainly constructed through the aggregation of monomeric hairpins. Thus, one can evaluate the entropy of each conformation by counting how many conformations can be built that belong to a particular cluster.

One possible arrangement consists of hairpins in a planar conformation, such as the ones reported in Fig. 3. As explained above, these conformations have many constraints on how the charges are packed, so their entropy is generally very low. However, the formation of hydrogen bonds leads to a lower energy as well. Conformations corresponding to cluster A (i.e., with two hairpins in a tilted conformation) allow for a much higher entropy because the two hairpins can either slide or flip with respect to each other. Extended conformations have more favorable energetic contributions than the hairpins as a result of more favorable hydrogen bonding between the strands, and because an extended chain intrinsically has a lower energy (primarily as a result of its dihedral angles) (39). Clusters of type C (consisting of a hairpin and a distorted hairpin) take advantage of both energetic and entropic stabilizations. The fact that one stem of one hairpin forms hydrogen bonds with the other hairpin results in lower energy, whereas the dangling sections of the chain allows multiple conformations to be adopted. Hence, it is not surprising that compact conformations with a tilted hairpin (such as cluster A) or with a dangling section (such as cluster C) are the most stable due to entropic considerations.

## Trimer: extended β-sheet conformations dominate the conformational space

In the trimer, there is an obvious transition from compact to extended structures, as shown in Fig. 1 c, which depicts the distribution of a single chain inside the trimer. We denote these new populations in the plot as T1, T2, and T3. These conformations are more extended than those seen in the dimer case. Although structure T3 is not highly populated, it represents a fully stretched chain and can be considered as an upper limit for the chain extension.

Overall, the trimers do not seem to adopt a preferential structure, and instead populate multiple aggregate conformations, as can be seen from both Fig. 1 (one chain inside the trimers) and Fig. 2 b (overall trimers conformations). The most populated clusters are composed of extended chains, such as clusters A and B. Cluster A has a β-sheet conformation with antiparallel alignment of the chains, with the plane slightly twisted along the directions of the hydrogen bonds (Fig. S13). Planar β-sheet conformations are not optimal conformations because they expose the hydrophobic moieties to the solvent, and the aggregates therefore tend to adopt conformations that can minimize this type of exposure. Cluster B shows another possible means of protecting the hydrophobic side chains by twisting the backbones to achieve a more compact structure.

Of interest, trimers also populate aggregates composed of both β-hairpins and extended chains. These aggregates are fundamental for understanding how β-hairpins, which are commonly found in monomers in solution, become incorporated inside a growing fibril. Consider, for instance, cluster C, which consists of two stretched chains and one chain in a hairpin-like conformation. The hairpin does not form intramolecular hydrogen bonds (required to become a proper β-hairpin), but rather forms intermolecular hydrogen bonds with the stretched chains. This arrangement suggests that a β-hairpin conformation is destabilized in the presence of two straight chains. However, the inclusion of a β-hairpin inside a trimer leads to more subtle effects on the structure of the oligomer. Indeed, we have found that flat oligomers are usually formed by extended chains with a hairpin at one of the edges, such as those found in cluster F. If all the chains are extended, the plane with the hydrogen bonds is usually distorted to better protect the hydrophobic moieties, as in clusters A and B.

A general feature shared by all the chains is that they are disposed in an antiparallel fashion, a consequence of the electrostatic considerations discussed in the previous section in the context of the dimer. Slight out-of-registry arrangements (see cluster A) are observed. In general, structures composed only of β-hairpins are scarce, and we only observe trimers of distorted hairpins in our simulations (such as those found in cluster D, with three bent chains clustered together). It is clear that, even in this conformation, the chains prefer to form interchain hydrogen bonds as in cluster C. Clusters with all three chains in a compact hairpin conformation are rare. In particular, we have not found any flat conformations composed only by β-hairpins, with arrangements similar to what was found for the dimers (for example, clusters F and H in Fig. 3).

In general, the trimer shows a more complicated behavior than the dimer. The structures of the dimer can be predicted mainly on the basis of electrostatic arguments. However, in the case of the trimer, electrostatic interactions would drive toward extended conformations, subsequently exposing a large hydrophobic surface. In the case of the dimer,

electrostatics is sufficient to counterbalance the hydrophobic effect, whereas this is not the case for the trimer. In the trimer, the structures try to optimize the surface area to minimize the hydrophobic surface (driving to compact conformations), whereas the electrostatic interactions tend to keep the sections of the chains as far apart as possible to minimize the repulsion between charges (driving to extended conformations). The chains hence tend to become stretched to optimize the charge repulsions, and the stretched chains in turn allow for better packing of the hydrophobic lateral groups as well.

## Tetramer: extended chains dominate

The tetramers show a better-defined structure than the trimers, even though a certain degree of heterogeneity is still present. In the case of the trimers, this heterogeneity is a consequence of the fact that single chains can adopt both extended and hairpin conformations. In contrast, the chain inside a tetramer favors a stretched conformation (Fig. 1 d), and the heterogeneity is a consequence of the different possible ways to organize these chains (Fig. 2 c). Tetramers tend to prefer compact conformations to minimize the exposed hydrophobic surface. A clear example of this is cluster A. The chains are stretched, with the hydrophobic side chains packed inside. In this arrangement, the chains are also able to build favorable interchain hydrogen bonds. This structure resembles a β-barrel, with a shape similar to that of a chalice. Chains adopt an antiparallel arrangement as in the trimer. This β-barrel conformation is intriguing in light of the hypothesis that the toxicity of Aβ(25–35) is connected to the formation of transmembrane voltage-dependent ion channels that can alter normal cell homeostasis (14,19,85). In a previous study, Kim and Weaver (85) used MD simulations to build model pores. They showed that Aβ(25–35) can form cylindrical aggregates with an internal cavity that potentially can transfer ions through the membrane. These aggregates were composed of Aβ(25–35) peptides in an extended conformation kept together by hydrogen bonds among the backbones. These structures are very similar to the distorted β-barrel conformations adopted by the tetramers in our simulations. In a recent study by Laganowsky et al. (86), the formation of β-barrel structures (named cylindrins) during aggregation was confirmed. These species were shown to be toxic, highlighting the importance of gaining a better understanding of the aggregates that are off-pathways to the formation of fibrils. Clusters B and C are representative of the majority of the clusters found, and account for the most-compact structures. Because the chains in these clusters do not form as many hydrogen bonds as in cluster A, they can slide with respect to each other and form more compact, spherical-like aggregates.

In general, chains tend not to form β-hairpins; rather, they try to be extended to form as many hydrogen bonds as possible. These resulting conformations are very compact, to protect the hydrophobic core. A notable exception is cluster D. This cluster is particularly interesting because, unlike the clusters described above, it adopts a flat conformation with two hairpins at the edges. In this arrangement, the chains can maximize both intra- and interchain hydrogen bonds, while at the same time the hydrophobic side chains are clustered together in a small region. In contrast, as can be seen in cluster I, when the chains are all extended, the plane tends to be twisted to maximize the hydrophobic contacts (Fig. S13). This is similar to what was observed for the trimer, suggesting once again that flat extended structures require the recruitment of hairpins (the most common monomer structure present in solution) at their edges to avoid distortion of the β-sheet and its collapse into more compact conformations. Such conformations can better protect the hydrophobic moieties, but are less likely candidates for further fibril formation.

In sum, the tetramer case starts to show an obvious predominance of hydrophobic effect over electrostatic repulsion. This is likely a result of the abundance of stretched chains that keep the charges farther apart than in the case of the dimer. It is important to emphasize that trimers and tetramers show similar trends. For example, both oligomers tend to allow for a variety of structures, ranging from compact structures to extended ones. Compact structures can be explained in terms of minimizing the (hydrophobic) surface area, whereas extended structures show a more complicated behavior. In fact, the presence of a hairpin at one extremity of the β-sheet leads the sheet to have a flatter conformation. In this respect, the trimer represents the transition point toward fibrillar-like structures. In fact, as the oligomer size increases, hairpins are increasingly disfavored, so that hairpins included in a β-sheet are very likely destabilized, leading to their extension and the resulting growth of the sheet.

## DISCUSSION AND CONCLUSIONS

Our simulations show that the Aβ(25–35) peptide undergoes a major structural rearrangement when moving from a dimer to a trimer. This transition is characterized by a switch from β-hairpin conformations to β-strands. The extension of the chains is mainly related to the problem of packing the charged groups along the backbone of each peptide in an efficient way. We also found that β-sheets are in equilibrium with more-compact structures, such that the distribution of conformations for trimers and tetramers is extremely heterogeneous. Whereas the formation of compact structures can be explained on the basis of minimizing the exposure of hydrophobic moieties, as will be explained below, the stabilization of β-sheets is probably driven by kinetic considerations rather than equilibrium ones.

Even though REMD does not allow for a direct probing of the kinetics, we can draw some conclusions about the most

likely growth pathways based on the structures found in our study (Fig. 4). One of the models that has been proposed in the literature to explain the aggregation of amyloids is a two-step mechanism (87,88) in the spirit of the dock-lock model proposed by Esler and co-workers (89). In the first step, the chains collapse driven by hydrophobic interactions. After this collapse occurs, the aggregate starts to rearrange itself to improve the packing of the chains. In this second stage of aggregation, the chains try to maximize the number of interchain hydrogen bonds. As a consequence, they adopt a stretched conformation and form $\beta$-sheet structures. This mechanism was observed by Cheon et al. (88) in simulations of the aggregation pathway of A$\beta$(16–22), but it does not appear to be the case for A$\beta$(25–35). Rather, we observe in our simulations that the initial oligomers try to properly pack the charged residues, very often exposing their hydrophobic moieties, in contrast with what would be expected in a hydrophobic collapse. In particular, the structures that are most likely to grow into fibrils show the highest exposure.

Our simulations suggest an alternate view of aggregation that draws from crystallization processes. It is well known that in the case of synthetic polymers, such as polyethylene, the growth of crystalline structures is of a kinetic rather than an equilibrium nature. This means that the crystalline structure that is obtained is the one that has a faster growth rate, and this does not typically correspond to the equilibrium structure (90).

The process we have in mind is sketched in Fig. 4. The aggregation starts with the association of two $\beta$-hairpins, the most common conformation for monomers is solution. At this stage, as discussed for the dimers, one of the chains is usually destabilized and adopts an extended conformation. A third incoming chain would stick to the extended chain of the dimer and as a consequence extend as well. This process will eventually continue until a stable fibril is grown.
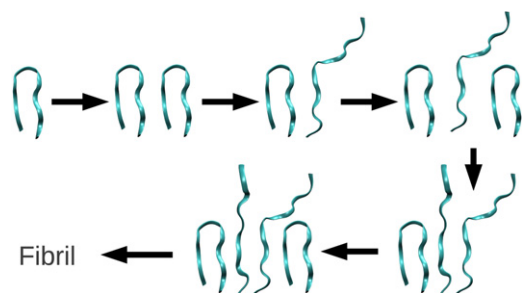


FIGURE 4 Proposed aggregation pathway. The aggregation is triggered by the association of two monomers in a $\beta$-hairpin conformation. At this point, one of the two chains is usually destabilized and adopts an extended conformation. In the same way, other monomers can be added to the growing front. Of interest, when all of the chains are extended, the oligomers tend to form compact conformations instead of a flat $\beta$-sheet. Thus, a flux of incoming $\beta$-hairpins is necessary to avoid this collapse, making this a kinetic (rather than an equilibrium) growth model.

In principle, there are a number of ways by which the propagation process could proceed. In one scenario, all of the $\beta$-hairpins would extend at the same time. These types of extended oligomers are indeed present in our simulations (for example, cluster B for the dimers), but are never the dominant conformation. Even though these structures appear to have the correct structure to grow into fibrils, they tend to buckle, and eventually collapse into a more compact structure (a good example is cluster A for the tetramers). As a consequence, these $\beta$-sheet conformations are unlikely candidates as seeds for further aggregation into fibrils. Instead, our simulations show that more plausible precursors for aggregation are trimers and tetramers that adopt structures with a chain in a hairpin conformation or with a floating chain-end at one end of the sheet (a good example is cluster F for the trimer; Fig. 2). Our simulations indicate that before they are destabilized, $\beta$-hairpins help ensure a flat conformation of the $\beta$-sheet adjoining the hairpin (see discussion about tetramers). Thus, not only is the hairpin monomer essential for the growth process, it is also required for the structural stabilization of the $\beta$-sheet. In another scenario, an extra chain enters a dimer formed by two proper hairpins. We do not believe that this is a likely growth mechanism, because this type of aggregate requires a longer time to reorganize, as both an extension and a relocation of the chains are required.

In summary, our simulations support a picture in which the growth of the fibril is dictated by the ability of the hairpin to first stabilize a flat, $\beta$-sheet conformation, and then to be destabilized in a second step so as to form an extended chain. The importance of kinetically stable structures for the formation of amyloid was also observed in MD simulations by Hwang et al. (91), in which dimeric conformations were seen to be kinetically trapped long enough for other chains to add to the aggregate. In the context of larger aggregates than the ones studied here, simulations by Magno and co-workers (92) showed the dependence of fibril formation on the stability of the $\beta$-sheet structures formed.

The importance of $\beta$-hairpin formation for fibril growth can be inferred from experiments that influence the hairpin population. Our simulations show that the charged states of the termini play a critical role in the formation of the hairpin. In particular, both K28 and M35 are key players in this respect. When a single chain is considered, K28 competes with the N-terminus for the negatively charged C-terminus (see discussion about the monomers). On the other hand, when multiple chains come close together, the electrostatic repulsion of the lysines plays a key role in shaping the final stable conformation(s) (a detailed discussion about this effect can be found in the section about dimers). Terzi et al. (34) showed that as the pH of a solution of A$\beta$(25–35) is lowered from pH 7.4 to pH 4.0 or 5.5, leading to a less charged C-terminus, the equilibrium is shifted away from a $\beta$ structure toward a random coil

conformation. Consistently, only stable insoluble amyloid aggregates are found when incubated at pH 7.4 (93). Experiments have also shown that mutations of the terminal methionine M35 group (the latter being associated with Aβ aggregate oxidative stress) to lysine can block the aggregation process (14,19,26). Replacing M35 by aspartate, on the other hand, promotes aggregation. Our simulations provide an explanation for these observations. Indeed, a lysine at the C-terminus will repeal the N-terminus, abolishing the formation of a β-hairpin and disfavoring aggregation. In addition, an extra lysine will double the total charge per chain, increasing the repulsion among the different chains. Following the same line of reasoning, aspartate with its negative charge will have the exact opposite effect.

The ability of the peptide backbone to switch among different conformations (i.e., from hairpin to extended) requires an intrinsic flexibility of the side chains. In fact, if the barrier for the transition from β-hairpin to β-strand is too high, the aggregation process will be slowed down considerably. Experimental support for this picture can be found in the work of Pike and co-workers (26), which showed that mutating M35 into a less flexible amino acid, such as leucine or tyrosine, hampers or even fully blocks aggregation.

The view that we propose is consistent with a previous theoretical study by Ma and Nussinov (94), which showed that the stability of monomeric intermediate species can affect the growth of fibrils of Aβ(25–35).

Our model is also compatible with the dock-lock mechanism proposed in the literature (89,95–99), in which the monomer adds to the growing front in a dock phase, followed by a structural rearrangement that locks the newly added chain into position. As in the dock-lock model, our model agrees with the experimental finding that the lock phase is the rate-limiting process (89,100). Our model has the unique feature that the most stable conformations do not consist of pure β-sheets; rather, they either contain hairpins or are formed from compact aggregates of β-strands. Our model relies on a very specific conformation (the hairpin) that is destabilized when it is in contact with other chains, leading it to adopt a β-strand conformation. A more detailed discussion of our model is given in Fig. S14. At the same time, this model reconciles the observation that although hairpins are present in the monomer form, they do not appear in the context of full-fledged fibrils, which consist primarily of extended (or, for some sequences, strand-loop-strand) motifs. It also explains why experiments that force the formation of overly stable β-hairpins in the monomeric state by means such as disulfide bonds (e.g., the Aβ$_{40}$ cc and Aβ$_{42}$ cc constructs of Sandberg et al. (47)) actually lead to decreased fibril formation and to the population of other types of aggregates. Our simulations highlight the fact that the hairpin needs to retain sufficient flexibility so that it can readjust its structure to accommodate the fibril structure, which an overly stable conformation

(such as a disulfide-linked hairpin) would not be able do. It is interesting to contrast the cross-linking procedure of Sandberg et al. (47), in which a hairpin structure (i.e., a conformation not present in the fibril) was enforced in Aβ, with the cross-linking performed by Sciarretta et al. (101). In the latter study, residues D23–K28, which are located in the loop region of Aβ in the context of the fibril, were cross-linked via a lactam bridge. As a result of this modification, the monomeric peptide preferentially adopted a conformation that was already commensurate with the strand-loop-strand conformations found in the fibril, leading to a significant increase in Aβ aggregation rates.

## SUPPORTING MATERIAL

Details about simulations protocol and convergence, extra pictures, abundance of each cluster, and reference (102) are available at www.biophys.org/biophysj/supplemental/S0006-3495(12)00716-3.

## REFERENCES

1. Dobson, C. M. 1999. Protein misfolding, evolution and disease. *Trends Biochem. Sci.* 24:329–332.

2. Fink, A. L. 1998. Protein aggregation: folding aggregates, inclusion bodies and amyloid. *Fold. Des.* 3:R9–R23.

3. Chiti, F., and C. M. Dobson. 2006. Protein misfolding, functional amyloid, and human disease. *Annu. Rev. Biochem.* 75:333–366.

4. Maji, S. K., L. Wang, …, R. Riek. 2009. Structure-activity relationship of amyloid fibrils. *FEBS Lett.* 583:2610–2617.

5. Bucciantini, M., E. Giannoni, …, M. Stefani. 2002. Inherent toxicity of aggregates implies a common mechanism for protein misfolding diseases. *Nature.* 416:507–511.

6. Bieschke, J., S. J. Siegel, …, J. W. Kelly. 2008. Alzheimer's Aβ peptides containing an isostructural backbone mutation afford distinct aggregate morphologies but analogous cytotoxicity. Evidence for a common low-abundance toxic structure(s)? *Biochemistry.* 47:50–59.

7. Stefani, M. 2007. Generic cell dysfunction in neurodegenerative disorders: role of surfaces in early protein misfolding, aggregation, and aggregate cytotoxicity. *Neuroscientist.* 13:519–531.

8. Baglioni, S., F. Casamenti, …, M. Stefani. 2006. Prefibrillar amyloid aggregates could be generic toxins in higher organisms. *J. Neurosci.* 26:8160–8167.

9. Petkova, A. T., R. D. Leapman, …, R. Tycko. 2005. Self-propagating, molecular-level polymorphism in Alzheimer's β-amyloid fibrils. *Science.* 307:262–265.

10. Alzheimer, A. 1907. Uber eine eigenartige Erkrankung der Hirnrinde. *Allg. Zeitschr. Psychiatr.* 64:146–148.

11. Hardy, J., and D. J. Selkoe. 2002. The amyloid hypothesis of Alzheimer's disease: progress and problems on the road to therapeutics. *Science*. 297:353–356.

12. Kang, J., H.-G. Lemaire, …, B. Müller-Hill. 1987. The precursor of Alzheimer's disease amyloid A4 protein resembles a cell-surface receptor. *Nature*. 325:733–736.

13. Nunan, J., and D. H. Small. 2000. Regulation of APP cleavage by $\alpha$-, $\beta$- and $\gamma$-secretases. *FEBS Lett*. 483:6–10.

14. Kaminsky, Y. G., M. W. Marlatt, …, E. A. Kosenko. 2010. Subcellular and metabolic examination of amyloid-$\beta$ peptides in Alzheimer disease pathogenesis: evidence for A$\beta$(25-35). *Exp. Neurol*. 221:26–37.

15. Pike, C. J., D. Burdick, …, C. W. Cotman. 1993. Neurodegeneration induced by $\beta$-amyloid peptides in vitro: the role of peptide assembly state. *J. Neurosci*. 13:1676–1687.

16. Frautschy, S. A., A. Baird, and G. M. Cole. 1991. Effects of injected Alzheimer $\beta$-amyloid cores in rat brain. *Proc. Natl. Acad. Sci. USA*. 88:8362–8366.

17. Ross, C. A., and M. A. Poirier. 2005. Opinion: What is the role of protein aggregation in neurodegeneration? *Nat. Rev. Mol. Cell Biol*. 6:891–898.

18. Cleary, J. P., D. M. Walsh, …, K. H. Ashe. 2005. Natural oligomers of the amyloid-$\beta$ protein specifically disrupt cognitive function. *Nat. Neurosci*. 8:79–84.

19. Millucci, L., L. Ghezzi, …, A. Santucci. 2010. Conformations and biological activities of amyloid $\beta$ peptide 25-35. *Curr. Protein Pept. Sci*. 11:54–67.

20. Roher, A. E., J. D. Lowenson, …, M. J. Ball. 1993. Structural alterations in the peptide backbone of $\beta$-amyloid core protein may account for its deposition and stability in Alzheimer's disease. *J. Biol. Chem*. 268:3072–3083.

21. Kubo, T., S. Nishimura, …, I. Kaneko. 2002. In vivo conversion of racemized $\beta$-amyloid ([D-Ser $^{26}$]A$\beta$ 1-40) to truncated and toxic fragments ([D-Ser $^{26}$]A$\beta$ 25-35/40) and fragment presence in the brains of Alzheimer's patients. *J. Neurosci. Res*. 70:474–483.

22. Stepanichev, M. Y., Y. V. Moiseeva, …, N. V. Gulyaeva. 2005. Studies of the effects of fragment (25-35) of $\beta$-amyloid peptide on the behavior of rats in a radial maze. *Neurosci. Behav. Physiol*. 35:511–518.

23. Stepanichev, M. Y., I. M. Zdobnova, …, N. V. Gulyaeva. 2006. Studies of the effects of central administration of $\beta$-amyloid peptide (25-35): pathomorphological changes in the hippocampus and impairment of spatial memory. *Neurosci. Behav. Physiol*. 36:101–106.

24. Limón, I. D., A. Díaz, …, J. Guevara. 2009. Amyloid-$\beta$(25-35) impairs memory and increases NO in the temporal cortex of rats. *Neurosci. Res*. 63:129–137.

25. Fraser, P. E., L. K. Duffy, …, D. A. Kirschner. 1991. Morphology and antibody recognition of synthetic $\beta$-amyloid peptides. *J. Neurosci. Res*. 28:474–485.

26. Pike, C. J., A. J. Walencewicz-Wasserman, …, C. W. Cotman. 1995. Structure-activity analyses of $\beta$-amyloid peptides: contributions of the $\beta$ 25-35 region to aggregation and neurotoxicity. *J. Neurochem*. 64:253–265.

27. Kaneko, I., N. Yamada, …, S. Tutumi. 1995. Suppression of mitochondrial succinate dehydrogenase, a primary target of $\beta$-amyloid, and its derivative racemized at Ser residue. *J. Neurochem*. 65:2585–2593.

28. el-Agnaf, O. M. A., G. B. Irvine, and D. J. S. Guthrie. 1997. Conformations of $\beta$-amyloid in solution. *J. Neurochem*. 68:437–439.

29. Misiti, F., B. Sampaolese, …, M. E. Clementi. 2005. A$\beta$(31-35) peptide induce apoptosis in PC 12 cells: contrast with A$\beta$(25-35) peptide and examination of underlying mechanisms. *Neurochem. Int*. 46:575–583.

30. Clementi, M. E., S. Marini, …, F. Misiti. 2005. A$\beta$(31-35) and A$\beta$(25-35) fragments of amyloid $\beta$-protein induce cellular death through apoptotic signals: Role of the redox state of methionine-35. *FEBS Lett*. 579:2913–2918.

31. Buchét, R., E. Tavitian, …, D. A. Lowe. 1996. Conformations of synthetic $\beta$ peptides in solid state and in aqueous solution: relation to toxicity in PC12 cells. *Biochim. Biophys. Acta*. 1315:40–46.

32. Kohno, T., K. Kobayashi, …, A. Takashima. 1996. Three-dimensional structures of the amyloid $\beta$ peptide (25-35) in membrane-mimicking environment. *Biochemistry*. 35:16094–16104.

33. D'Ursi, A. M., M. R. Armenante, …, D. Picone. 2004. Solution structure of amyloid $\beta$-peptide (25-35) in different media. *J. Med. Chem*. 47:4231–4238.

34. Terzi, E., G. Hölzemann, and J. Seelig. 1994. Reversible random coil-$\beta$-sheet transition of the Alzheimer $\beta$-amyloid fragment (25-35). *Biochemistry*. 33:1345–1350.

35. Terzi, E., G. Hölzemann, and J. Seelig. 1994. Alzheimer $\beta$-amyloid peptide 25-35: electrostatic interactions with phospholipid membranes. *Biochemistry*. 33:7434–7441.

36. Shanmugam, G., and P. L. Polavarapu. 2004. Structure of A$\beta$(25-35) peptide in different environments. *Biophys. J*. 87:622–630.

37. Wei, G., and J.-E. Shea. 2006. Effects of solvent on the structure of the Alzheimer amyloid-$\beta$(25-35) peptide. *Biophys. J*. 91:1638–1647.

38. Wei, G., A. I. Jewett, and J.-E. Shea. 2010. Structural diversity of dimers of the Alzheimer amyloid-$\beta$(25-35) peptide and polymorphism of the resulting fibrils. *Phys. Chem. Chem. Phys*. 12:3622–3629.

39. Kittner, M., and V. Knecht. 2010. Disordered versus fibril-like amyloid $\beta$ (25-35) dimers in water: structure and thermodynamics. *J. Phys. Chem. B*. 114:15288–15295.

40. Dupuis, N. F., C. Wu, …, M. T. Bowers. 2011. The amyloid formation mechanism in human IAPP: dimers have $\beta$-strand monomer-monomer interfaces. *J. Am. Chem. Soc*. 133:7240–7243.

41. Dupuis, N. F., C. Wu, …, M. T. Bowers. 2009. Human islet amyloid polypeptide monomers form ordered $\beta$-hairpins: a possible direct amyloidogenic precursor. *J. Am. Chem. Soc*. 131:18283–18292.

42. Baumketner, A., M. G. Krone, and J.-E. Shea. 2008. Role of the familial Dutch mutation E22Q in the folding and aggregation of the 15-28 fragment of the Alzheimer amyloid-$\beta$ protein. *Proc. Natl. Acad. Sci. USA*. 105:6027–6032.

43. Baumketner, A., and J.-E. Shea. 2007. The structure of the Alzheimer amyloid $\beta$ 10-35 peptide probed through replica-exchange molecular dynamics simulations in explicit solvent. *J. Mol. Biol*. 366:275–285.

44. Baumketner, A., and J.-E. Shea. 2006. Folding landscapes of the Alzheimer amyloid-$\beta$(12-28) peptide. *J. Mol. Biol*. 362:567–579.

45. Grabenauer, M., C. Wu, …, M. T. Bowers. 2010. Oligomers of the prion protein fragment 106-126 are likely assembled from $\beta$-hairpins in solution, and methionine oxidation inhibits assembly without altering the peptide's monomeric conformation. *J. Am. Chem. Soc*. 132:532–539.

46. Härd, T. 2011. Protein engineering to stabilize soluble amyloid $\beta$-protein aggregates for structural and functional studies. *FEBS J*. 278:3884–3892.

47. Sandberg, A., L. M. Luheshi, …, T. Härd. 2010. Stabilization of neurotoxic Alzheimer amyloid-$\beta$ oligomers by protein engineering. *Proc. Natl. Acad. Sci. USA*. 107:15595–15600.

48. Yu, L., R. Edalji, …, E. T. Olejniczak. 2009. Structural characterization of a soluble amyloid $\beta$-peptide oligomer. *Biochemistry*. 48:1870–1877.

49. Hoyer, W., C. Grönwall, …, T. Härd. 2008. Stabilization of a $\beta$-hairpin in monomeric Alzheimer's amyloid-$\beta$ peptide inhibits amyloid formation. *Proc. Natl. Acad. Sci. USA*. 105:5099–5104.

50. Hoyer, W., and T. Härd. 2008. Interaction of Alzheimer's A$\beta$ peptide with an engineered binding protein—thermodynamics and kinetics of coupled folding-binding. *J. Mol. Biol*. 378:398–411.

51. Hou, L., H. Shao, …, M. G. Zagorski. 2004. Solution NMR studies of the A$\beta$(1-40) and A$\beta$(1-42) peptides establish that the Met35

oxidation state affects the mechanism of amyloid formation. *J. Am. Chem. Soc.* 126:1992–2005.

52. Lazo, N. D., M. A. Grant, …, D. B. Teplow. 2005. On the nucleation of amyloid β-protein monomer folding. *Protein Sci.* 14:1581–1596.

53. Mitternacht, S., I. Staneva, …, A. Irbäck. 2010. Comparing the folding free-energy landscapes of Aβ42 variants with different aggregation properties. *Proteins.* 78:2600–2608.

54. Yang, M., and D. B. Teplow. 2008. Amyloid β-protein monomer folding: free-energy surfaces reveal alloform-specific differences. *J. Mol. Biol.* 384:450–464.

55. Habicht, G., C. Haupt, …, M. Fändrich. 2007. Directed selection of a conformational antibody domain that prevents mature amyloid fibril formation by stabilizing Aβ protofibrils. *Proc. Natl. Acad. Sci. USA.* 104:19232–19237.

56. Cerf, E., R. Sarroukh, …, V. Raussens. 2009. Antiparallel β-sheet: a signature structure of the oligomeric amyloid β-peptide. *Biochem. J.* 421:415–423.

57. Daidone, I., A. Di Nola, and J. C. Smith. 2011. Molecular origin of Gerstmann-Sträussler-Scheinker syndrome: insight from computer simulation of an amyloidogenic prion peptide. *Biophys. J.* 100:3000–3007.

58. Reddy, A. S., L. Wang, …, J. J. de Pablo. 2010. Stable and metastable states of human amylin in solution. *Biophys. J.* 99:2208–2216.

59. Itoh, S. G., and Y. Okamoto. 2008. Amyloid-β(29-42) dimer formations studied by a multicanonical-multioverlap molecular dynamics simulation. *J. Phys. Chem. B.* 112:2767–2770.

60. Lu, Y., G. Wei, and P. Derreumaux. 2011. Effects of G33A and G33I mutations on the structures of monomer and dimer of the amyloid-β fragment 29-42 by replica exchange molecular dynamics simulations. *J. Phys. Chem. B.* 115:1282–1288.

61. Lu, Y., P. Derreumaux, …, G. Wei. 2009. Thermodynamics and dynamics of amyloid peptide oligomerization are sequence dependent. *Proteins.* 75:954–963.

62. Simona, F., G. Tiana, …, G. Colombo. 2004. Modeling the α-helix to β-hairpin transition mechanism and the formation of oligomeric aggregates of the fibrillogenic peptide Aβ(12-28): insights from all-atom molecular dynamics simulations. *J. Mol. Graph. Model.* 23:263–273.

63. Daidone, I., F. Simona, …, A. Di Nola. 2004. β-Hairpin conformation of fibrillogenic peptides: structure and α-β transition mechanism revealed by molecular dynamics simulations. *Proteins.* 57:198–204.

64. Hess, B., C. Kutzner, …, E. Lindahl. 2008. GROMACS 4: algorithms for highly efficient, load-balanced, and scalable molecular simulation. *J. Chem. Theory Comput.* 4:435–447.

65. Van Der Spoel, D., E. Lindahl, …, H. J. Berendsen. 2005. GROMACS: fast, flexible, and free. *J. Comput. Chem.* 26:1701–1718.

66. Lindahl, E., B. Hess, and D. van der Spoel. 2001. GROMACS 3.0: a package for molecular simulation and trajectory analysis. *J. Mol. Model.* 7:306–317.

67. Berendsen, H. J. C., D. van der Spoel, and R. van Drunen. 1995. GROMACS: a message-passing parallel molecular dynamics implementation. *Comput. Phys. Commun.* 91:43–56.

68. Jorgensen, W. L., D. S. Maxwell, and J. Tirado-Rives. 1996. Development and testing of the OPLS all-atom force field on conformational energetics and properties of organic liquids. *J. Am. Chem. Soc.* 118:11225–11236.

69. Rizzo, R. C., and W. L. Jorgensen. 1999. OPLS all-atom model for amines: resolution of the amine hydration problem. *J. Am. Chem. Soc.* 121:4827–4836.

70. Kaminski, G. A., R. Friesner, …, W. Jorgensen. 2001. Evaluation and reparametrization of the OPLS-AA force field for proteins via comparison with accurate quantum chemical calculations on peptides. *J. Phys. Chem. B.* 105:6474–6487.

71. Jorgensen, W. L., J. Chandrasekhar, …, M. L. Klein. 1983. Comparison of simple potential functions for simulating liquid water. *J. Chem. Phys.* 79:926–935.

72. Darden, T., D. York, and L. Pedersen. 1993. Particle mesh Ewald: an N · log(N) method for Ewald sums in large systems. *J. Chem. Phys.* 98:10089–10092.

73. Essman, U., L. Perela, …, L. G. Pedersen. 1995. A smooth particle mesh Ewald method. *J. Chem. Phys.* 103:8577–8592.

74. Nosé, S. 1984. A molecular dynamics method for simulations in the canonical ensemble. *Mol. Phys.* 52:255–268.

75. Nosé, S. 1984. A unified formulation of the constant temperature molecular dynamics methods. *J. Chem. Phys.* 81:511–519.

76. Hoover, W. G. 1985. Canonical dynamics: Equilibrium phase-space distributions. *Phys. Rev. A.* 31:1695–1697.

77. Verlet, L. 1967. Computer "experiments" on classical fluids. I. Thermodynamical properties of Lennard-Jones molecules. *Phys. Rev.* 159:98–103.

78. Hess, B., H. Bekker, …, J. G. E. M. Fraaije. 1997. LINCS: a linear constraint solver for molecular simulations. *J. Comput. Chem.* 18:1463–1472.

79. Miyamoto, S., and P. A. Kollman. 1992. Settle: An analytical version of the SHAKE and RATTLE algorithm for rigid water models. *J. Comput. Chem.* 13:952–962.

80. Hukushima, K., and K. Nemoto. 1996. Exchange Monte Carlo method and application to spin glass simulations. *J. Phys. Soc. Jpn.* 65:1604–1608.

81. Sugita, Y., and Y. Okamoto. 1999. Replica-exchange molecular dynamics method for protein folding. *Chem. Phys. Lett.* 314:141–151.

82. Patriksson, A., and D. van der Spoel. 2008. A temperature predictor for parallel tempering simulations. *Phys. Chem. Chem. Phys.* 10:2073–2077.

83. Daura, X., K. Gademann, …, A. E. Mark. 1999. Peptide folding: when simulation meets experiment. *Angew. Chem. Int. Ed.* 38:236–240.

84. Strobl, G. R. 2007. The Physics of Polymers, 3rd ed. Springer, New York.

85. Kim, S., and D. Weaver. 2000. Theoretical studies on Alzheimer's disease: structures of β-amyloid aggregates. *Theochem.* 527:127–138.

86. Laganowsky, A., C. Liu, …, D. Eisenberg. 2012. Atomic view of a toxic amyloid small oligomer. *Science.* 335:1228–1231.

87. Serio, T. R., A. G. Cashikar, …, S. L. Lindquist. 2000. Nucleated conformational conversion and the replication of conformational information by a prion determinant. *Science.* 289:1317–1321.

88. Cheon, M., I. Chang, …, G. Favrin. 2007. Structural reorganisation and potential toxicity of oligomeric species formed during the assembly of amyloid fibrils. *PLOS Comput. Biol.* 3:1727–1738.

89. Esler, W. P., E. R. Stimson, …, J. E. Maggio. 2000. Alzheimer's disease amyloid propagation by a template-dependent dock-lock mechanism. *Biochemistry.* 39:6288–6295.

90. Armitstead, K., G. Goldbeck-Wood, and A. Keller. 1992. Polymer crystallization theories. *Adv. Polym. Sci.* 100:219–312.

91. Hwang, W., S. Zhang, …, M. Karplus. 2004. Kinetic control of dimer structure formation in amyloid fibrillogenesis. *Proc. Natl. Acad. Sci. USA.* 101:12916–12921.

92. Magno, A., R. Pellarin, and A. Caflisch. 2012. Mechanisms and kinetics of amyloid aggregation investigated by a phenomenological coarse-grained model. *In* Computational Modeling of Biological Systems. Biological and Medical Physics, Biomedical Engineering. N. Dokholyan, editor. Springer, New York. 191–214.

93. Millucci, L., R. Raggiaschi, …, A. Santucci. 2009. Rapid aggregation and assembly in aqueous solution of A β (25-35) peptide. *J. Biosci.* 34:293–303.

94. Ma, B., and R. Nussinov. 2006. The stability of monomeric intermediates controls amyloid formation: Aβ25-35 and its N27Q mutant. *Biophys. J.* 90:3365–3374.

95. Massi, F., and J. E. Straub. 2001. Energy landscape theory for Alzheimer's amyloid β-peptide fibril elongation. *Proteins.* 42:217–229.

96. Straub, J. E., and D. Thirumalai. 2011. Toward a molecular theory of early and late events in monomer to amyloid fibril formation. *Annu. Rev. Phys. Chem.* 62:437–463.

97. Takeda, T., and D. K. Klimov. 2009. Replica exchange simulations of the thermodynamics of Aβ fibril growth. *Biophys. J.* 96:442–452.

98. O'Brien, E. P., Y. Okamoto, …, D. Thirumalai. 2009. Thermodynamic perspective on the dock-lock growth mechanism of amyloid fibrils. *J. Phys. Chem. B.* 113:14421–14430.

99. Nguyen, P. H., M. S. Li, …, D. Thirumalai. 2007. Monomer adds to preformed structured oligomers of Aβ-peptides by a two-stage dock-lock mechanism. *Proc. Natl. Acad. Sci. USA.* 104:111–116.

100. Cannon, M. J., A. D. Williams, …, D. G. Myszka. 2004. Kinetic analysis of β-amyloid fibril elongation. *Anal. Biochem.* 328:67–75.

101. Sciarretta, K. L., D. J. Gordon, …, S. C. Meredith. 2005. Aβ40-Lactam(D23/K28) models a conformation highly favorable for nucleation of amyloid. *Biochemistry.* 44:6003–6014.

102. Hansen, J.-P., and I. R. McDonald. 2006. Theory of Simple Liquids, 3rd ed. Academic Press, New York.